

INSTRUMENTATION

Theoretical Studies of Image Artifacts and Counting Losses for Different Photon Fluence Rates and Pulse-Height Distributions in Single-Crystal NaI(Tl) Scintillation Cameras

Sven-Erik Strand and Inger-Lena Lamm

Department of Radiation Physics, Lund University Hospital, Lund, Sweden

Using computer simulations, we have developed a theoretical model to explain the correlation between counting losses and image artifacts in single-crystal NaI(Tl) scintillation cameras. The theory, valid for scintillation cameras of the Anger type, is based on the physical properties of the NaI(Tl) crystal. Based on a statistical model using random numbers, pulse trains of the light pulses from scintillations were simulated. Pulse-height distributions for different event rates were calculated, with various Compton distributions. Images of point sources and line sources were generated. Counting losses and image artifacts were dependent on the shape of the pulse-height distribution. The calculated counting losses decreased with larger Compton distributions, due to increasing numbers of pileup events in the energy window; this also caused severe image distortion. The improvement of the spatial resolution with pileup rejection was demonstrated. The theoretical results are in good agreement with experimental results obtained previously.

It is concluded that, in modern cameras, the decay time of the scintillation determines the amount of pileup, and the resolving time of the electronics governs the count rates. The results indicate that in some modern cameras the limits of the count-rate capacity in Anger cameras may be reached.

J Nucl Med 21: 264-275, 1980

Rapid biological processes are nowadays studied more and more with radioactive tracers and scintillation-camera imaging. To collect enough events during short time intervals, high activities must be used. In nuclear cardiology, for example, activities of Tc-99m in the range 0.35-1.0 GBq (10-30 mCi) are frequently needed. In emission computerized tomography with scintillation cameras, high activities might also be used (1-3).

When a single-crystal NaI(Tl) scintillation camera is exposed to high photon fluence rates, the counting losses become considerable. In addition, pileup of pulses

may occur, leading to a deterioration in the quality of the image due to wrongly positioned events.

The importance of a reliable assessment of the count-rate capacity of a scintillation camera, enabling a clear distinction to be made between correctly and falsely positioned events, has been demonstrated in earlier works from this department (4-7). Similar studies elsewhere have also shown the correlation between counting losses and image distortion (8-13). These papers explicitly—and others (14-18) indirectly—show that the counting rate is determined by the total photon fluence rate impinging on the NaI(Tl) crystal and not by the registered counting rate in the energy window.

No theoretical evaluation of the correlation between counting losses and image artifacts in Anger scintillation cameras has yet been published. The aim of the present

Received Feb. 23, 1979; revision accepted Oct. 10, 1979.

For reprints contact: Sven-Erik Strand, PhD, Radiation Physics Dept., Lasarettet, S-221 85 Lund, Sweden.

investigation is to present such a theory and to compare it with experimental results.

THEORY

Scintillation-camera pulse arithmetic. This general theory deals with the physical properties of the NaI(Tl) crystal. When photons interact with a NaI(Tl) crystal, usually 13 mm thick in Anger cameras, scintillations are produced. The light has a rise time of 60 nsec and decreases with decay times of 0.23 μ sec for 60% of the light pulse and 1.15 μ sec for the remainder (19, 20). Consider the typical train of events shown in Fig. 1. Let a photon generate a light pulse, W_0 , in the crystal. After a time T_1 , the next photon produces a pulse, W_1 , while a residual portion, U_1 , from pulse W_0 still remains, and so on. In the general case, when the n th light pulse, W_n , is created a time T_n after the $(n - 1)$ th light pulse, the light remaining from all the preceding events is U_n .

In a scintillation camera, the positioning signals, X_n and Y_n , are generated simultaneously. These signals are proportional to the position of the photon event in the crystal times the photon energy dissipated, and must therefore be divided by the "energy signal," Z_n , to give the energy-independent position signals X'_n and Y'_n (20, 21). Assuming that the pulses decay exponentially with decay time TK, the equations for the three signals Z_n , X'_n , and Y'_n describing the n th event become

$$Z_n = W_n + U_n = W_n + Z_{n-1} \exp(-T_n/TK) \quad (1)$$

$$X'_n = \frac{X_n + X_{n-1} \cdot \exp(-T_n/TK)}{Z_n} \quad (2)$$

$$Y'_n = \frac{Y_n + Y_{n-1} \cdot \exp(-T_n/TK)}{Z_n} \quad (3)$$

All events in the crystal generate these signals, but only those events whose pulse heights, Z_n , fall within the

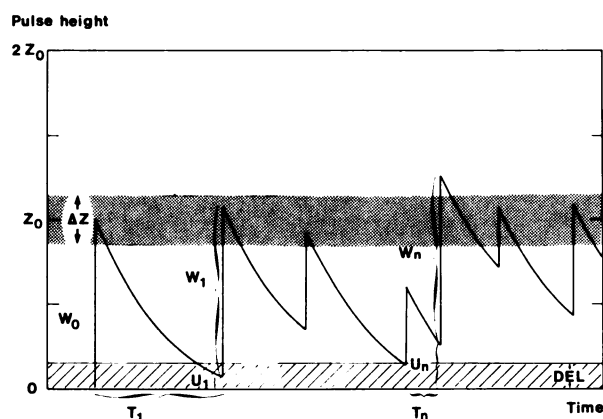


FIG. 1. Pulse train with full-energy pulse height, Z_0 , generated theoretically. Also indicated are pulse-height window, ΔZ , and pileup-rejection level, DEL.

pulse-height window, ΔZ , around Z_0 are recorded (Fig. 1). This is the same as the condition:

$$|Z_n - Z_0| \leq 1/2 \cdot \Delta Z \quad (4)$$

Misplaced events will occur when an event takes place before earlier signals have almost completely decayed, and also when two or more events, each with energy too small to be detected separately, fall within a time interval small enough for the sum of the Z -signals to be accepted in the window (pulse pileup).

The actual degree of faulty placement can be still larger if in the electric circuitry the positioning signals are summed on the tails of the earlier voltage signals. In some modern cameras this is avoided by buffering the signals (22). Further improvement is achieved when pulse-pileup rejection is applied (22), reducing the relative number of misplaced events.

MATHEMATICAL MODEL

Time interval between interactions. The time interval, T , between consecutive scintillations in the NaI(Tl)-crystal, caused by the interactions of the photons, is exponentially distributed (23). The intensity of the scintillation light was idealized assuming that all pulses have zero rise time and an exponential decay with decay time TK. In the theoretical calculations, the times of arrival of photons in terms of the time intervals, T , between events are needed, and it can be shown (see Appendix) that, using the uniformly distributed random number, $\bar{\xi}$, the relative decay of a pulse during time T is given by

$$\exp(-T/TK) = \bar{\xi}^{1/(TK \cdot IA)} \quad (5)$$

where IA is the event rate in the crystal. The product $TK \cdot IA$ determines the probability for pulse pileup. In Table 1, the values of the event rate IA are given, for several values of the product $TK \cdot IA$, for two relevant decay times (0.2 μ sec and 1 μ sec).

Interactions in the crystal: monoenergetic source in air. If the photon source emits monoenergetic photons of energy E_0 , and is situated in air, essentially all the photons reaching the crystal have energy E_0 . For monoenergetic photons interacting in the crystal, either total absorption or partial absorption (due to Compton effect) of the photon energy occurs. The pulse height corresponding to full-energy absorption is denoted by Z_0 .

In this so-called "air case," the pulse-height distribution due to partially absorbed photons, the "Compton distribution," is approximated by a uniform distribution from zero energy up to a maximum energy, E_C , the Compton edge, given by

$$E_C = \frac{E_0}{1 + \frac{m_0 c^2}{2E_0}} \quad m_0 c^2 = 511 \text{ keV} \quad (6)$$

TABLE 1. THE EVENT RATE, IA, FOR DIFFERENT VALUES OF THE PRODUCT OF DECAY TIME AND EVENT RATE, TK·IA

TK·IA	Event rate, sec ⁻¹	
	TK = 0.2 μsec	TK = 1.0 μsec
10 ⁻⁴	5·10 ²	10 ²
10 ⁻³	5·10 ³	10 ³
10 ⁻²	5·10 ⁴	10 ⁴
10 ⁻¹	5·10 ⁵	10 ⁵
10 ⁰	5·10 ⁶	10 ⁶

The fraction of events in the Compton distribution is denoted by C, and hence the fraction of full-energy events is (1 - C). The details are described in the Appendix, which also includes a description of the simulation of a pulse train using uniformly distributed random numbers.

Interactions in the crystal: monoenergetic source in a scattering medium. When a monoenergetic emitter is immersed in a scattering medium, the so-called "water case," the photons impinging on the crystal are no longer monoenergetic, but include a continuous energy distribution of photons singly or repeatedly scattered. The pulse-height distribution resulting from a continuous distribution of impinging photons will also show a continuous distribution, from zero to Z₀, the full-energy pulse height.

The effects of the interactions in both the crystal and the scattering medium are approximated in the calculations by using a pulse-height distribution trapezoidal

in form between zero and Z₀ and a spike at Z₀, corresponding to the full-energy events. This pulse-height distribution is simulated using the uniformly distributed random numbers mentioned earlier, the details being included in the Appendix.

Pileup rejection. Modern scintillation cameras are equipped with some kind of pileup-rejection circuit. The details of these differ for different types of cameras, but their main purpose is to remove the summed pulses. In the theoretical treatment, a pileup-rejection level (denoted by DEL) was introduced such that for a light pulse, W, occurring when the residual light signal, U, was greater than the selected rejection level,

$$U \geq \text{DEL} \tag{7}$$

the corresponding event was not recorded (Fig. 1).

Simulated images. Two source geometries were simulated (Fig. 2). The first consisted of four point sources situated at the corners of a square, and was the same as that used in our earlier experiments (4-6). Images of parallel line sources with decreasing separation were also generated and were chosen to investigate the influence of different event rates on spatial resolution. The coordinates for photon events creating the images of the sources were simulated by random numbers.

Computer simulations. The theoretical model described above was written as a FORTRAN IV program and the simulations were performed on a laboratory computer. The images of the sources were generated by pulses, Z_n, accepted in the pulse-height window, ΔZ, and not rejected by the pileup rejection condition if pileup rejection were used.

THE FACTOR, DECAY TIME×EVENT RATE, TK·IA

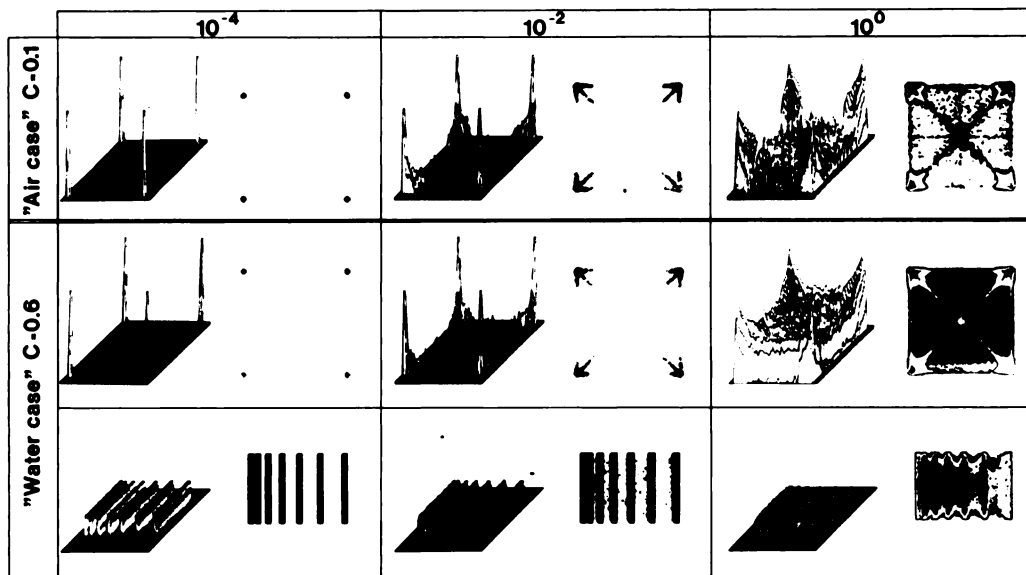


FIG. 2. Volumetric and 2-cycle gray-scale displays (semilog) of simulated four point sources for "air case" and "water case." Images are shown for TK·IA = 10⁻⁴, 10⁻², and 10⁰. For "water case", parallel line sources are also simulated. No pileup rejection is used.

The evaluation of the results for the images of the four point sources used the same technique as that described in Ref. 6. Thus, a region of interest between the four sources in a shape of a "cross" was selected. Inside this cross, the pulses in the theoretical treatment are due only to pileup.

As a measure of image distortion, an index, R, was defined (6) as

$$R = \frac{\text{count rate outside the cross}}{\text{total count rate in image}} \quad (8)$$

It was also possible to calculate exactly the numbers of events that were correctly placed in the images of the sources, corresponding count rates being denoted by "Events in source."

RESULTS

Pulse-height distributions. Examples of some simu-

lated pulse-height distributions are given in Fig. 3 for both the "air case" and the "water case." In the "air case" in which monoenergetic photons impinge on the crystal, the value $C = 0.1$ is used for the Compton fraction. This is a realistic figure for the 140-keV photons from Tc-99m, and means that 10% of the events registered in the crystal lead to partial absorption and 90% to total absorption of the photon energy. In this figure, the value $C = 0.4$ is chosen for the "water case," where as mentioned above the continuous part of the pulse-height distribution takes into account both the continuous nature of the photon spectrum and the interactions in the crystal. The number of full-energy events is thus 40% of the total number of events. The value of C is related to the scattering conditions, as shown previously (6).

Results are shown for values of 10^{-4} , 10^{-1} , and 10^0 of the product $TK \cdot IA$, the decay time times event rate. The higher the event rate, the greater the distortion of

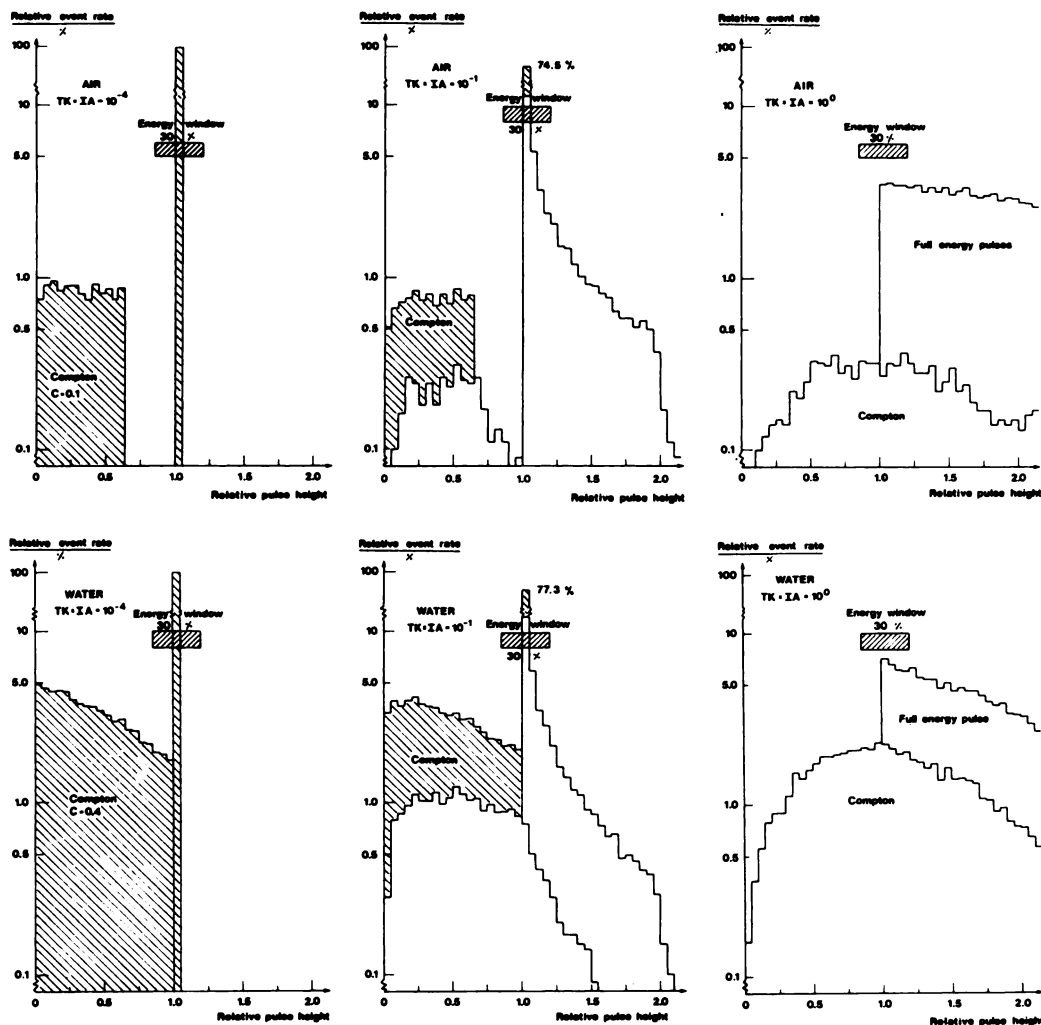


FIG 3. Simulated pulse-height distributions for "air case" with $C = 0.1$ and "water case" with $C = 0.6$. Examples with product $TK \cdot IA = 10^{-4}$, 10^{-1} , and 10^0 are given. A 30% pulse-height window is indicated. Shaded areas represent pulses accepted if pileup-rejection level (DEL) is $0.01 \cdot Z_0$; and unshaded areas indicate pileup pulses.

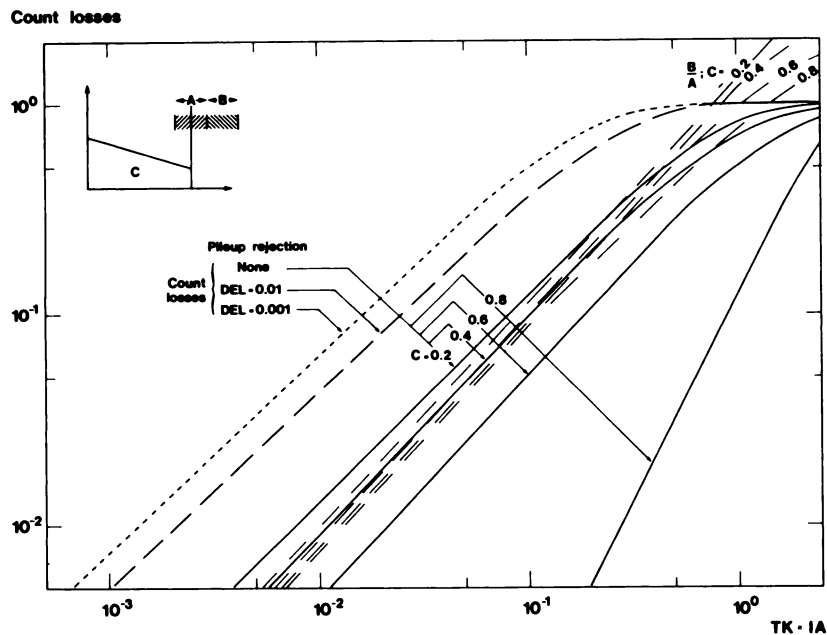


FIG. 4. Count losses calculated for a 30% energy window centered over full-energy pulse-height position, as a function of the product TK·IA for C = 0.2, 0.4, 0.6, and 0.8. Effect of pileup rejection on count losses is shown for two pileup-rejection levels, 0.01·Z₀ and 0.001·Z₀. Ratios of count rate in a higher pulse-height window, B (see insert), to count rate in original window, A, are shown as dashed lines.

the pulse-height distribution. In the figures, a 30% energy window centred around the full-energy pulse-height, Z₀, is indicated. Depending mainly on the fraction of events in the Compton distribution, an increasing number of pileup pulses will fall within this window, increasing the event rate. The greater the Compton distribution, the greater the number of pileup pulses generated. In the diagram, the hatched areas represent the fraction of pulses accepted when a pileup-rejection level, DEL = 0.01·Z₀, is chosen. Further calculations with other shapes of the Compton distribution have shown that the results given in this work concerning the influence on pileup were dependent mainly on the number of events in the Compton distribution and only to a minor extent on the specific shape of this distribution.

The influence of pileup events was further demonstrated when counting losses in the 30% energy window were studied. The count losses, defined as

$$\text{Count losses} = 1 - \frac{\text{"measured" count rate}}{\text{expected count rate}} \quad (9)$$

are plotted as a function of the product TK·IA in Fig. 4 for the "water case" with Compton fractions 0.2, 0.4, 0.6, and 0.8. The smaller the Compton distribution, the greater the apparent counting losses due to the decreasing number of pileup pulses that fall within the window. To show the effect of pileup rejection, the counting losses for rejection levels of 0.01·Z₀ and 0.001·Z₀ are also given. When pileup rejection was used, the largest counting losses were found for the smallest values of the rejection level (DEL) and there was no noticeable influence of the fraction of events in the Compton distribution.

Also indicated in this figure (dashed lines) is the ratio

of the counting rate in a pulse-height window, B, just above the usual one, A, (see insert in Fig. 4) to the counting rate in window A. This ratio has an almost linear dependence on the counting rate, and varies only slightly with the fraction of events in the Compton distribution. The occurrence of a linear relationship of this type has been shown experimentally earlier (24).

Simulated images. In Fig. 2 the digital images of the simulated four point sources and line sources are displayed as volumetric (35) or 2-cycle gray-scale (26) images. The effect of the product TK·IA on the images is demonstrated in Fig. 2 for the values 10⁻⁴, 10⁻², and 10⁰. A Compton fraction of 10% (C = 0.1), was used for the "air case" and 60% (C = 0.6), for the "water case" (6).

It is obvious from Fig. 2 that, in addition to the original sources, some artifacts are also present in the simulated images. These false events are positioned closer to the source in the "air case" and extend farther out between the sources in the "water case," in which photons are scattered within the source. With larger Compton distributions, the probability increases for coincidences of two or more photons scattered from different regions, in which case the resulting pileup pulse is accepted in the pulse-height window and positioned somewhere between the sources. For smaller Compton distributions, most of the pileup pulses in the window are due to full-energy pulses, each superimposed on the tail of a previous one and causing only a slight misplacement, if any.

Pileup events in the image were evaluated by summing the events in the "cross" mentioned earlier, and in Fig. 5A, values of the index R for different relative widths, Δl/l, of this cross are listed. The value of R decreases when the width increases, since the cross will cover areas with increasing numbers of slightly misplaced events.

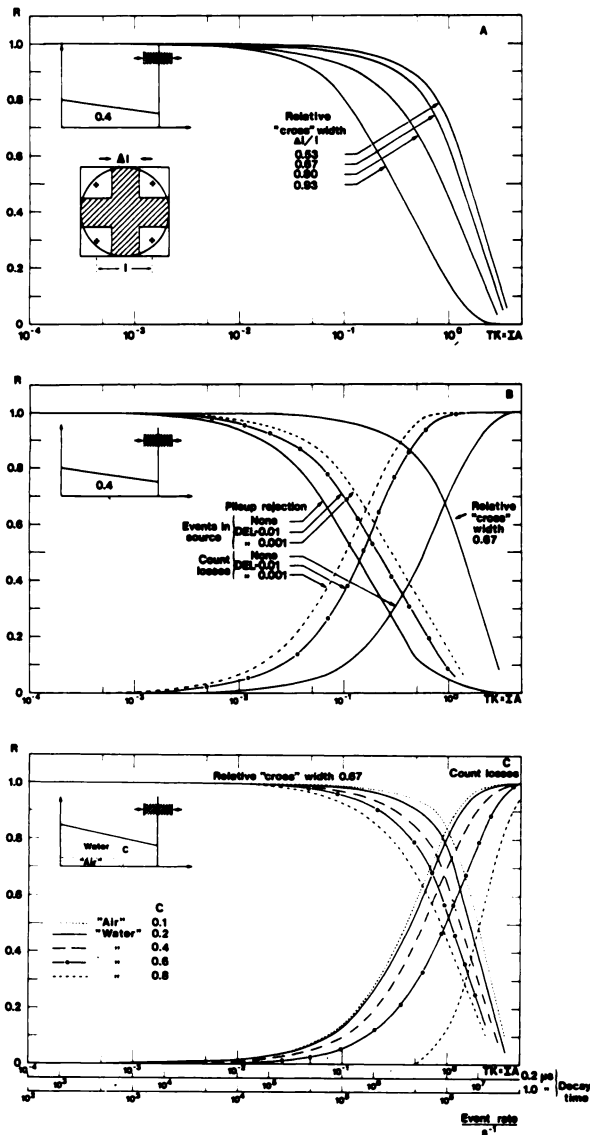


FIG. 5. Fraction of total events in simulated image of four sources registered with 30% pulse-height window, plotted against product $TK \cdot IA$. (A) "With right position" outside the "cross", i.e., index R, for different widths of cross. (B) Correctly positioned within sources ("Events in source"), together with counting losses for pileup-rejection levels of $0.001 \cdot Z_0$, $0.01 \cdot Z_0$, and ∞ . For comparison, curve with relative cross width 0.67 from A, above, is included. (C) Index R for different values of fraction of events in Compton distribution, together with count losses for "air case" and "water case."

The count rates within the images of the four sources were calculated. These values are given in Fig. 5 B as fractions of the counting rate in the total image ("Events in source"), with and without pileup rejection at $DEL = 0.01 \cdot Z_0$ and $0.001 \cdot Z_0$, together with the R values for the cross with relative width 0.67. Also included in the figure are the corresponding counting losses. The data are for the "water case" with a Compton fraction $C = 0.6$ and a 30% pulse-height window. The values determined for the "Events in source" are much lower than the R values

calculated with the "cross" technique because, in the former, values for only a few slightly misplaced events are included, whereas in the latter such events are much more frequent. With pileup rejection, the fraction of correctly placed events increases due to exclusion of the false events, the exclusion being greater the smaller the pileup-rejection level used. The fraction of the total events correctly placed in the image ("Events in source") was found to be almost independent of the fraction of events in the Compton distribution.

Counting losses increase when pileup rejection is applied, but this is accompanied by increased reliability of the image information. In Table 2, the fraction of events with "right position" ("cross" technique) and events with "true position" ("Events in source") are given for counting losses of 10, 30, and 50% for different pulse-height distributions. From this it is seen that specifying the count-rate capacity of a scintillation camera only as the value of the counting losses is quite insufficient: the recorded events must be useful events and not pileup pulses degrading the image information. The number of misplaced events is strongly dependent on the fraction of events in the Compton distribution. In Fig. 5C the change in the number of misplaced events in the cross is given, with varying amounts of scattering, together with the counting losses. The fraction of the total events in the image positioned outside the cross (index R) decreases when the relative number of events in the Compton distribution, C, increases, because of the increased number of pileup pulses recorded in the window, as mentioned earlier. Furthermore, the larger the number of pileup pulses recorded, the smaller the apparent counting losses. At the foot of Fig. 5, the values of the corresponding event rates, IA are given for the decay times ($0.2 \mu\text{sec}$ and $1 \mu\text{sec}$) used in Table 1.

Count-rate curves. In Fig. 6 the counting rates that might be observed in a 30% pulse-height window are plotted as a function of the expected counting rate in that window for the "water case," with $C = 0.6$. The fraction of the total event rate, IA, within the pulse-height window, giving the expected counting rate, has been calculated for a value of $0.2 \mu\text{sec}$ for the decay time TK.

The curves in Fig. 6 A show the counting rates that could be measured in the camera if all events could be processed without any losses in the pulse-handling circuitry. These curves thus show the optimal count-rate capacity obtainable with the large NaI(Tl) crystals in scintillation cameras with the assumptions used in the above theory. The same technique for evaluating the images of the four sources as used experimentally in Ref. 6 was simulated. Thus with the same nomenclature as in Ref. 6, the "Total" counting rate in the whole image, the counting rate outside a cross with relative width 0.67 (designated "With right position"), and the counting rate inside the cross ("Pileup") have been calculated. The patterns of the curves in Fig. 6 A are the same as the

TABLE 2. THE FRACTION OF THE TOTAL NUMBER OF EVENTS IN THE IMAGE OF THE FOUR POINT SOURCES WITH "RIGHT" ("CROSS" TECHNIQUE) AND "TRUE" ("EVENTS IN SOURCE") POSITIONS

Theoretical model	Fraction of event rate, C, in Compton distribution	"Right position"			"True position"		
		Count losses (%)			Count losses (%)		
		10	30	50	10	30	50
"Air"	0.1	0.99	0.98	0.96	0.68	0.46	0.18
"Water"	0.2	0.98	0.96	0.92	0.64	0.30	0.15
	0.4	0.97	0.91	0.81	0.57	0.25	0.10
	0.6	0.92	0.76	0.56	0.39	0.10	0.04
	0.8	0.46	0.25	0.17	0.03	0.01	0
Pileup rejection							
DEL = 0.01·Z ₀		1.00	1.00	1.00	0.91	0.74	0.60
DEL = 0.001·Z ₀		1.00	1.00	1.00	0.96	0.87	0.75

results in Ref. 6 for a scintillation camera without pileup rejection.

The simulated counting rates, however, are ten times the experimental values. This can be accounted for by a resolving time, τ , of a few microseconds in the pulse-handling circuits. It was therefore assumed that a nonparalyzable resolving-time correction (23) should be applied to the theoretical count rates, which hitherto had taken only the properties of the NaI(Tl) crystal into consideration. The count rates were reduced by a factor, k , for the corresponding event rate, IA , in the total pulse-height distribution, k being given by:

$$k = \frac{1}{1 + IA \cdot \tau} \quad (10)$$

In Fig. 6 B, the same curves as in Fig. 6 A are shown, with a nonparalyzable resolving time, τ , of 1 μ sec. The total maximum counting rate now obtainable is 240,000/sec.

The counting rates of events in the images of the sources ("Events in source") were also calculated. These values start to decrease at expected counting rates of 10,000/sec. The maximum obtainable counting rate is 140,000/sec if only the decay time of the scintillations is considered, and falling to 80,000/sec if in addition a resolving time of 1 μ sec is applied.

The counting rates when pileup rejection was simulated are shown in Figs. 6, C and D. The first figure shows the maximum counting rates obtainable if only the NaI(Tl) crystal is concerned, while the second shows the same curves if a resolving time of 1 μ sec is assumed for the camera. Curves for a pileup-rejection level (DEL) of 0.001·Z₀ and 0.01·Z₀ are given, as are both the counting rates in the total image ("Total") and the event rate in the images of the sources ("Events in source"). The larger the number of pileup pulses rejected, the smaller the counting rate recorded. No false events can

be recorded in the cross, and only a small number of events are slightly misplaced.

With the simulated pileup rejection, the total maximum counting rates obtainable with zero resolving time were 140,000 and 200,000/sec, and with a resolving time of 1 μ sec were 80,000 and 100,000/sec. Corresponding values for the "Events in source" are 100,000 and 130,000/sec, and 65,000 and 75,000/sec. The count-rate curves decrease very rapidly at high event rates in the crystal, for then the probability of pileup becomes very large and most of the incoming events are rejected. This decrease at high counting rates is accounted for by the properties of the crystal only and is not attributed to any resolving time of the circuitry.

Spatial resolution. To show qualitatively the influence of different count rates on spatial resolution, profiles through the images of the line sources were generated. In Fig. 7 the results of these simulations are shown for the "air case" ($C = 0.1$) and the "water case" ($C = 0.6$). Examples are given for values of the product $TK \cdot IA$ equal to 10^{-4} , 10^{-2} , and 10^0 . Increase of this product decreases the resolution. Also, without pileup rejection the relative number of events in the Compton distribution affects the dependence on the counting rate. In the "water case," the degradation due to misplaced events in the image is more pronounced than in the "air case." The pileup rejection available in the simulations showed that the influence of the pulse-height distributions on the spatial resolution was eliminated.

The reduction in the relative number of misplaced events will obviously increase the spatial resolution, and this might be one of the factors explaining the improved spatial resolution of modern scintillation cameras over the older types, noticeable in clinical studies.

DISCUSSION

The model presented here has delivered simulations

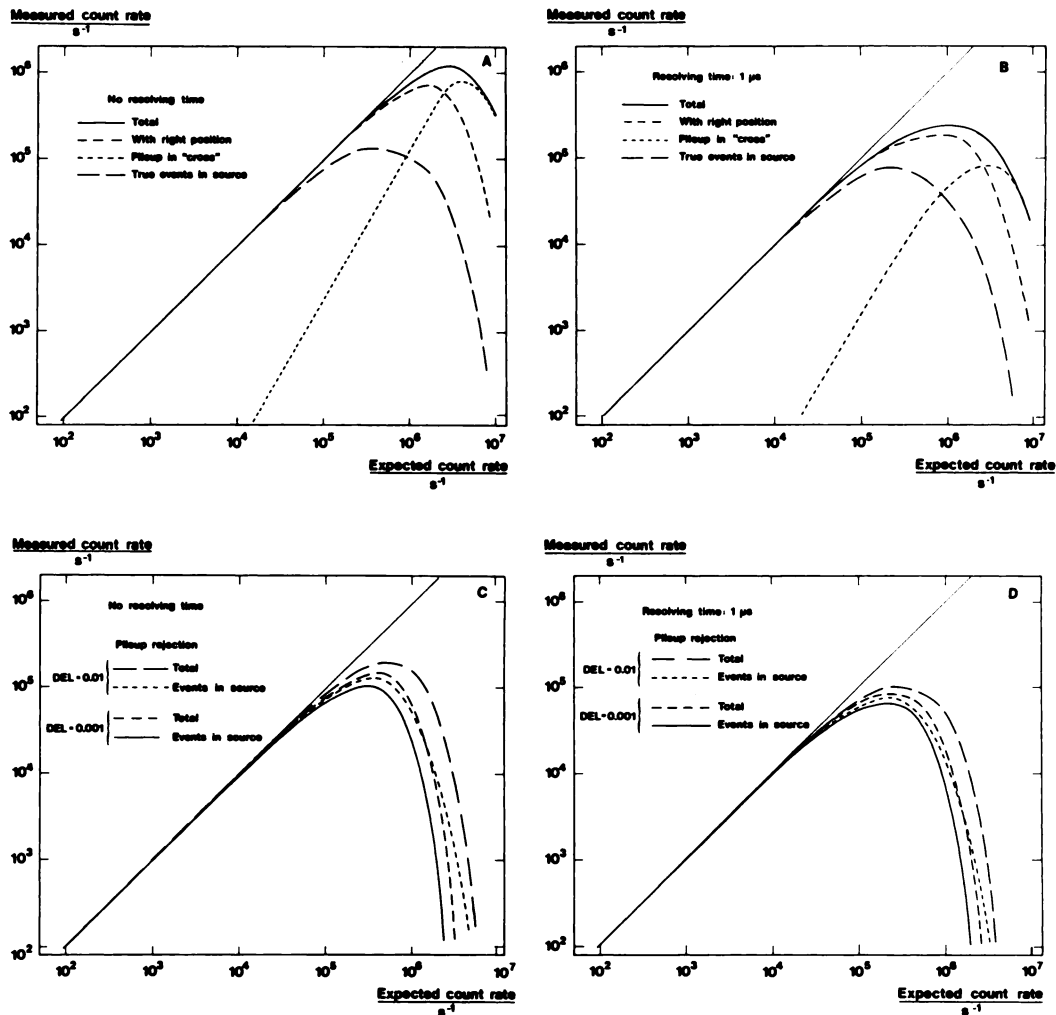


FIG. 6. Count-rate curves simulated for the four point sources with 30% pulse-height window for "water case," with $C = 0.6$. (A) Count rates in energy window if only a scintillation light decay time of $0.2 \mu\text{sec}$ is assumed. (B) Same curves as in A with additional assumption of nonparalyzable resolving time of $1 \mu\text{sec}$. (C) Same curves as in A but with pileup-rejection levels of $0.01 \cdot Z_0$ and $0.001 \cdot Z_0$. (D) Same curves as in C but with added resolving time of $1 \mu\text{sec}$.

of image artifacts and counting losses in single-crystal NaI(Tl) crystal scintillation cameras. The overall characteristics of the theoretical pulse-height distributions are in agreement with experimental data published by us (5, 6) and by others (8, 9, 24). By dividing the pileup pulses recorded within an energy window into summed Compton or full-energy pulses, the appearance of the image artifacts that have been found experimentally (4-6, 8-13, 24) under various conditions of scattering can be satisfactorily explained. Experimentally, several authors have reported (14, 18, 24, 27-33) that counting losses vary with scattering conditions and the width of the energy window, and have shown that the "dead time" of a scintillation camera varies with these parameters. It has been shown in our theoretical treatment that counting losses for a given scattering condition depend mainly on the total event rate in the crystal and only to a minor extent on the specific shape of the pulse-height distribution. Variations in apparent

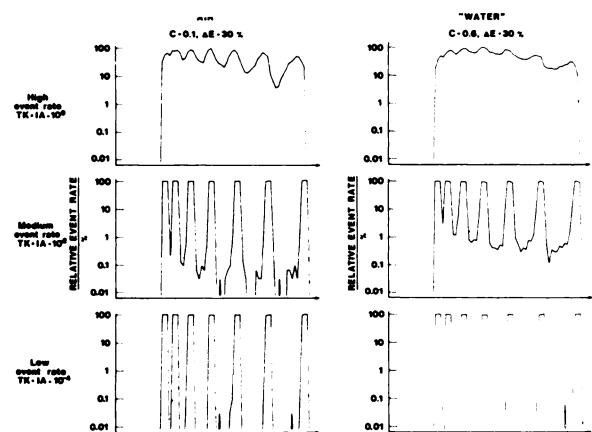


FIG. 7. Profiles through centers of simulated line sources for "air case" with $C = 0.1$, and "water case" with $C = 0.6$. Results are given for three values of product $TK \cdot IA$: 10^{-4} , 10^{-2} , and 10^0 . Note deterioration of spatial resolution with increasing event rate, due to misplaced events.

counting losses are due to the different numbers of true and pileup pulses recorded in the energy window chosen. The statement that the counting losses are determined by the overall shape of the total spectrum has been put forward by some authors (3-8, 16, 18, 33-35). The simulated theoretical values of the index R showed the same correlation with the shape of the pulse-height distribution as was obtained experimentally (4-6).

The degradation of spatial resolution at high count rates observed experimentally in different types of scintillation cameras (9, 10, 13, 36, 37) has been shown to agree with the theoretical results obtained here. In addition, it could also be shown theoretically that a major improvement in the quality of the image was achieved when pileup rejection was simulated in the images, both for the four point sources and the line sources. This effect of pileup rejection on the spatial resolution has been reported elsewhere (9, 13), the results being in agreement with the theory presented here. Rejection of the pileup pulses thus ensures improved digital information in the image.

The simulated count-rate curves showed the same characteristics as those obtained experimentally (6). Theoretically, with a given pulse-height window, the maximum obtainable counting rate that could be expected from scintillations in the NaI(Tl) crystal was estimated taking both true and false events into consideration and, if a nonparalyzable resolving-time correction was applied, good agreement between the theoretical and experimental count rates was found.

CONCLUSION

With a suitable theoretical model, simulations on a computer have made it possible to explain the causes of image artifacts and counting losses at different photon fluence rates in Anger scintillation cameras. The results are in good agreement with experimental data published earlier. The rate of photon interactions in the NaI(Tl) crystal determines the number of pileup pulses due to the decay time of the scintillation light, whereas the maximum obtainable counting rates in an energy window are limited by the resolving time of the camera's electronics.

That part of the total event rate generating the scintillation image is determined by the width of the pulse-height window. The number of pileup pulses falling within this window is related to the shape of the energy distribution of the photons. Counting losses and image artifacts thus vary with the amount of scattering material between source and detector. Rejection of the pileup pulses reduces this variation. Reliable measurements of the counting rate will be obtained only if adequate pileup rejection is applied to ensure that the measured count rate consists mainly of events correctly placed.

The theoretical calculations show that at expected

counting rates as low as 10,000/sec counting losses and image artifacts may appear. Taking into consideration only the decay time of the scintillation light in the NaI(Tl) crystal, the maximum obtainable counting rates for correctly positioned events are of the order of 150,000/sec. If, in addition, a resolving time of 1 μ sec in the circuitry is assumed, the maximum obtainable counting rates will be of the order of 100,000/sec. The results with simulated pileup rejection indicate that the count-rate capacities for some modern cameras—for example that shown for one of the cameras in Ref. 6—tend to approach the limits for single-crystal NaI(Tl) scintillation cameras while still maintaining good image quality.

ACKNOWLEDGMENTS

We thank C. J. Lamm for valuable discussions concerning the statistical treatment and I. Larsson for his fruitful criticism of the work. Thanks are also due to C. Lingårdh, who performed some of the simulations and prepared all the drawings, and to T. Gustafsson for the use of his computer programs to display our images.

This study was supported by grants from the John and Augusta Persson Foundation for Medical and Scientific Research, Lund, Sweden.

APPENDIX

Time intervals between consecutive registrations. The source used in the simulations is monoenergetic and emits photons that interact in some of the cases studied with a scattering medium before arriving at the detector. The photons are assumed to arrive in a Poisson stream and hence the time, T , between two consecutive arrivals is exponentially distributed, with distribution function

$$F_T(t) = \begin{cases} 0 & t < 0 \\ 1 - e^{-IA \cdot t} & t \geq 0 \end{cases} \quad (A1)$$

where IA is the event rate in the crystal.

The assumed simplified shape of the pulse from one registration is shown in Fig. 1, in which a pulse train is illustrated. The pulse rise time is assumed to be zero and the decay is exponential, with a decay time TK , where $TK = 1.44 T_{1/2}$. Pulses from adjacent events are assumed to add linearly.

Of interest here is to determine the amount of "tail" persisting from the previous pulses when the pulse of interest arrives. Thus the aim is to study the distribution of pulse heights registered at the times of photon arrival. As is easily seen from Fig. 1, the following relations apply:

$$\begin{aligned} U_1 &= W_0 \cdot e^{-T_1/TK} & \text{and } Z_1 &= W_1 + U_1; \\ U_2 &= W_0 \cdot e^{-(T_1+T_2)/TK} \\ &\quad + W_1 \cdot e^{-T_2/TK} \\ &= Z_1 \cdot e^{-T_2/TK} & \text{and } Z_2 &= W_2 + U_2 \\ &\vdots & & \vdots \\ U_n &= Z_{n-1} \cdot e^{-T_n/TK} & \text{and } Z_n &= W_n + U_n \end{aligned} \quad (A2)$$

The distribution of T is well known, but the distribution of $e^{-T/TK}$, the decay factor, is not known trivially. For simulation purposes, the stochastic variable $Q = e^{-T/TK}$ is conveniently generated as the transformation of a variable Ξ , uniformly distributed in the interval (0, 1), i.e., with distribution function

$$F_{\Xi}(\xi) = \begin{cases} 0 & \xi < 0 \\ \xi & 0 \leq \xi \leq 1 \\ 1 & \xi > 1 \end{cases} \quad (\text{A3})$$

The distribution function of Q, $F_Q(q)$, is by definition

$$F_Q(q) = P(Q \leq q). \quad (\text{A4})$$

Using the known properties of the variable T, the result becomes

$$F_Q(q) = q^{1A \cdot TK} \quad (\text{A5})$$

By making the transformation

$$V = \Xi^{1/(1A \cdot TK)} \quad (\text{A6})$$

a new variable, V, is created with a distribution function

$$F_V(v) = P(V \leq v) = v^{1A \cdot TK}. \quad (\text{A7})$$

The distribution functions of this transformed variable, V, and the variable Q are thus identical.

The computer used for the theoretical calculations contains a generator giving random numbers uniformly distributed in the interval (0, 1). Consequently, by applying the transformation defined above, the random-number generator will give random numbers $Q = e^{-T/TK}$ with the correct distribution function $F_Q(q)$. This technique is used in the theoretical study that is performed as a simulation of the real situation with random-number generation, first, of the decay factor $e^{-T/TK}$ and of the pulse-height registered; later, in the image-creation process, simulation of where the incident photon originated.

For a continuous stochastic variable, V, with distribution function F_V (and inverse F_V^{-1}), it can be shown generally that by putting

$$V = F_V^{-1}(\Xi), \quad (\text{A8})$$

the available uniformly distributed variable, Ξ , is transformed into the desired variable, V. This relation will be used in the following sections.

Pulse-height distributions. Interactions in the crystal: monoenergetic source in air. The monoenergetic photons, impinging on the crystal with energy E_0 , are either absorbed totally (giving full-energy events) or only partially due to the escape of Compton-scattered photons. In this "air case," the energy range covered by the partial-absorption events goes from zero up to E_C , the maximum energy of the Compton electrons (Eq. 6). In the model used here, this "Compton distribution" is approximated by a rectangular distribution from zero to E_C , containing a fraction, C, of the total number of registered events. Thus, the full-energy events constitute the fraction (1 - C). The energy, E, absorbed in the registration of a photon, is a stochastic variable with a frequency function $f_E(e)$, the energy spectrum, shown in Fig. 8. The distribution function, $F_E(e)$, also shown in Fig. 8, is given by

$$F_E(e) = \begin{cases} 0 & e < 0 \\ e \cdot \frac{C}{E_C} & 0 \leq e \leq E_C \\ C & E_C < e < E_0 \\ 1 & e \geq E_0 \end{cases} \quad (\text{A9})$$

By transforming the uniformly distributed stochastic variable, Ξ , available in the computer according to Eq. A8 using the distribution function in (A9), the result is the desired variable E:

$$E = \begin{cases} \frac{E_C}{C} \Xi & 0 \leq \Xi < C \\ E_0 & C \leq \Xi \leq 1 \end{cases} \quad (\text{A10})$$

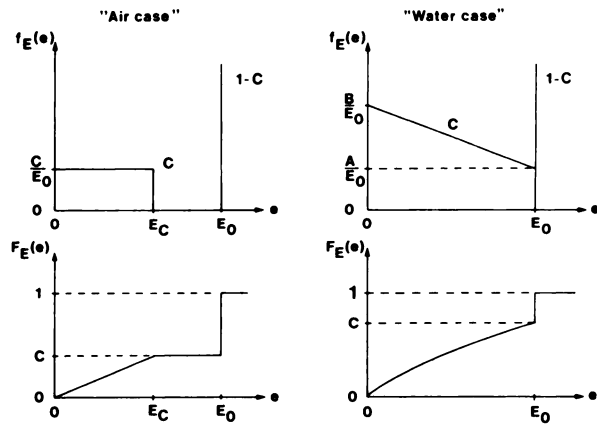


FIG. 8. Energy absorption in crystal due to emission of monoenergetic photons in source, frequency function $f_E(e)$ and distribution function $F_E(e)$ for "air case" and for "water case."

The stochastic variable W, the pulse height due to the interaction of a photon upon arrival, is simply proportional to E, the proportionality constant being Z_0/E_0 , where Z_0 is the pulse height corresponding to energy E_0 .

$$W = \frac{Z_0}{E_0} E = \begin{cases} \frac{Z_0}{E_0} \frac{E_C}{C} \Xi & 0 \leq \Xi < C \\ Z_0 & C \leq \Xi \leq 1 \end{cases} \quad (\text{A11})$$

The expected value of the total pulse height, Z, as measured exactly at the time of arrival of a photon, is denoted by m_Z . This value is used as the starting value of the pulse height in the simulations.

To get an expression of the expected pulse height, m_Z , it is useful to rewrite one of the equations in (A2).

$$Z_n = W_n + U_n = W_n + Z_{n-1} \cdot e^{-T_n/TK} \quad (\text{A12})$$

The expectation of this expression can be written as

$$E(Z_n) = E(W_n) + E(Z_{n-1}) \cdot E(e^{-T_n/TK}) \quad (\text{A12})$$

the variables Z and T being independent. The definition of expected value gives

$$E(e^{-T/TK}) = \int_{-\infty}^{\infty} f_T(t) e^{-t/TK} dt = \frac{1A \cdot TK}{1 + 1A \cdot TK} \quad (\text{A13})$$

For large values of n, i.e., large numbers of events, the expected values of both Z_n and Z_{n-1} tend toward the value m_Z , leading to the relation:

$$m_Z = \frac{Z_0}{E_0} E(e) + m_Z \frac{1A \cdot TK}{1 + 1A \cdot TK} \quad (\text{A14})$$

The expected value of the absorbed energy is easily calculated to be

$$E(e) = 0.5 C \cdot E_C + (1 - C) \cdot E_0 \quad (\text{A15})$$

which gives finally

$$m_Z = Z_0 \left(\frac{C}{2} \frac{E_C}{E_0} + (1 - C) \right) (1 + 1A \cdot TK) \quad (\text{A16})$$

To summarize, monoenergetic photons impinging with exponentially distributed time intervals on the model scintillation camera can be simulated on the computer using Eqs. A2 and A6. Each photon results in energy absorption in the crystal, described by the distribution function in (A9). This energy absorption leads to a pulse being generated, and the pulse height due to the ab-

sorption of a photon at the time of arrival is simulated on the computer using Eq. A11. In the simulation of a pulse train, the starting value of the pulse height is taken as the expected value of the registered pulse height at the time of arrival of the photons, given in Eq. A16.

Interactions in the crystal: monoenergetic source in a scattering medium. Next, consider the case when the monoenergetic source is surrounded by some scattering medium, the "water case." On account of the scattering processes in this medium, the photons impinging on the crystal will no longer be monoenergetic but will include a continuous distribution of photons.

To describe this situation, we used a simple approach in which a model of the pulse-height distribution was adopted. This distribution is supposed to include both the effects of the impinging continuous photon distribution and of the varying energy absorption distribution in the crystal.

The pulse-height distribution used is shown in Fig. 8 and the distribution function is given by

$$F_E(e) = \begin{cases} 0 & e < 0 \\ B \frac{e}{E_0} - \frac{e^2}{2E_0^2} (B - A) & 0 \leq e < E_0 \\ 1 & e \geq E_0 \end{cases} \quad (\text{A17})$$

As before, the fraction of partial-absorption events is denoted by C , the full-energy events constituting the fraction $(1 - C)$. This gives the following relation between the parameters A , B and C :

$$C = 0.5 (A + B) \quad (\text{A18})$$

In the transformation from the uniformly distributed variable, \bar{z} , to the absorbed energy E according to Eq. A8, using the distribution function (A17), three separate cases must be considered:

Case I: $A = B = C$

$$E = \begin{cases} \bar{z}/C & 0 \leq \bar{z} < C \\ 1 & C \leq \bar{z} \leq 1 \end{cases}$$

Case II: $B > A$

$$E = \begin{cases} \left(\frac{B}{B-A} - \left\{ \left(\frac{B}{B-A} \right)^2 - \frac{2\bar{z}}{B-A} \right\}^{1/2} \right) E_0 & 0 \leq \bar{z} < C \\ E_0 & C \leq \bar{z} \leq 1 \end{cases} \quad (\text{A19})$$

Case III: $B < A$

$$E = \begin{cases} \left(\frac{B}{B-A} + \left\{ \left(\frac{B}{B-A} \right)^2 - \frac{2\bar{z}}{B-A} \right\}^{1/2} \right) E_0 & 0 \leq \bar{z} < C \\ E_0 & C \leq \bar{z} \leq 1 \end{cases}$$

As in the former case, the expected value, m_z , of the pulse height, Z , registered at the time of arrival of the photons is used as the starting value in the simulation of a pulse train. For an arbitrary distribution of the energy absorbed in the registration of a photon, the following expression for m_z was deduced earlier (A14):

$$m_z = \frac{Z_0}{E_0} E(e) + m_z \frac{IA \cdot TK}{1 + IA \cdot TK} \quad (\text{A14})$$

The expected value $E(e)$ of the absorbed energy for the distribution used in the "water case" is

$$E(e) = E_0 \left(1 - \frac{B}{6} - \frac{C}{3} \right), \quad (\text{A20})$$

which results in the following expression:

$$m_z = z_0 \left(1 - \frac{B}{6} - \frac{C}{3} \right) (1 + IA \cdot TK) \quad (\text{A21})$$

Thus, the simulations of the two cases studied, the "air case" and the "water case," are performed similarly, the only difference being in the shape of the distribution of the energy absorbed in the crystal due to the emission of a monoenergetic photon from the source.

REFERENCES

1. BUDINGER TF, DERENZO SE, GREENBERG WL, et al: Quantitative potentials of dynamic emission computed tomography. *J Nucl Med* 19: 309-315, 1978
2. JASZCZAK RJ, MURPHY PH, HUARD D, et al: Radionuclide emission computed tomography of the head with ^{99m}Tc and a scintillation camera. *J Nucl Med* 18: 373-380, 1977
3. KEYES JW, ORLANDEA N, HEETDERKS WJ, et al: The humongotron—a scintillation-camera transaxial tomograph. *J Nucl Med* 18: 381-387, 1977
4. STRAND SE, LARSSON I: *Proceeding of Fifth Symposium on Medical Radionuclide Imaging*. Discussion. IAEA, 25-29 Oct., 1976, Los Angeles, pp 98-100
5. STRAND SE, LARSSON I, LAMM IL: Count losses and image distortion at high photon fluence rates (in Swedish). In *Proceeding of Swedish Association of Physicists in Medicine*, Ann. Meeting Stockholm, Sweden, Dec. 1976, p 294
6. STRAND S-E, LARSSON I: Image artifacts at high photon fluence rates in single-crystal NaI(Tl) scintillation cameras. *J Nucl Med* 19: 407-413, 1978
7. STRAND SE, LAMM IL: A theoretical model for the count losses and image distortion of the single-crystal scintillation camera at different photon fluence rates and energy spectra (in Swedish). In *Proceeding of Swedish Association of Physicists in Medicine*, Ann. Meeting Stockholm, Sweden, Nov. 1978, p 382
8. GULDBERG C, KARLE A, JØRGENSEN PB: Anger camera imaging of perfused and nonperfused brain tissue with intra-arterial ^{133}Xe technique. *Eur J Nucl Med* 2: 205-215, 1977
9. GULDBERG C, ROSSING N: Comparing the performance of two gamma cameras under high counting rates: principles and practice. *J Nucl Med* 19: 545-552, 1978
10. LANGE D, KOBER B, SCHENK P, et al: Totzeitverluste und pileup bei hohen Zaehlraten in Scintillationskamas. In *Radioactive Isotope in Klinik und Forschung*, Vienna. Höfer R, ed. Verlag H Egerman, 1976, pp 557-568
11. LANGE D, HERMANN HJ, WETZEL E, et al: Critical parameters to estimate the use of a scintillation camera in high dose dynamic studies. *Proceeding of Fifth Symposium on Medical Radionuclide Imaging*. IAEA, 25-29 Oct., 1976, Los Angeles, pp 85-97
12. LANGE D, HERMANN HJ, WETZEL E: Regional distribution of correction factors at high photon fluence rates—A definition for a "fast" scintillation camera. In *Radioaktive Isotope in Klinik und Forschung*, Vienna. Höfer R, ed. Verlag H Egerman, 1978, pp 321-332
13. MURPHY P, ARSENEAU R, MAXON E, et al: Clinical significance of scintillation camera electronics capable of high processing rates. *J Nucl Med* 18: 175-179, 1977
14. WICKS R, BLAU M: The effect of window fraction on the deadtime of Anger cameras: coincide communication. *J Nucl Med* 18: 732-735, 1977
15. MUEHILLEHNER G, JASZCZAK RJ, BECK RN: The reduction of coincidence loss in radionuclide imaging cameras through the use of composite filters. *Phys Med Biol* 19: 504-510, 1974
16. ADAM WE, BITTER F, KAMPMAN M, et al: Grundsätzliche Aspekte der Funktionsscintigraphie. *Proceedings of the International Annual Meeting of the Society of Nuclear*

- Medicine*, 10-13 Sept., 1975, Copenhagen, pp 180-193
17. IINUMA TA, FUKUHISA K, MATSUMOTO T, et al: Dynamic performance of scintillation camera - computer system and correction for counting-loss due to resolving time. *Proceedings of the First World Congress of Nuclear Medicine*, 30 Sept-4 Oct, 1974, Tokyo, pp 151-155
 18. ARNOLD JE, JOHNSTON AS, PINSKY SM: The influence of true counting rate and the photopeak fraction of detected events on Anger camera deadtime. *J Nucl Med* 15: 412-416, 1974
 19. BIRKS JB: *The Theory and Practice of Scintillation Counting*. Pergamon Press, Oxford, 1964, p 453
 20. HINE GJ: *Instrumentation in Nuclear Medicine*. Academic Press, New York, 1967, p 96
 21. ANGER HO: Sensitivity, resolution and linearity of the scintillation camera. *Trans Nucl Sci* 13: 380-392, 1966
 22. *PHO/GAMMA LFOV, PHO/GAMMA V, SERVICE MANUAL*, Searle Radiographics Inc., 1976, pp 5:1-5:7
 23. EVANS RD: *The Atomic Nucleus*, New York, McGraw-Hill, 1955, pp 753-754
 24. SORENSON JA: Methods of correcting Anger camera deadtime losses. *J Nucl Med* 17: 137-141, 1976
 25. MÖLLER T, GUSTAFSSON T, NAVERSTEN Y, et al: Computer evaluation of thyroid scans in clinical routine. In *Proceeding of Fourth Symposium on Medical Radioisotope Scintigraphy*. IAEA, 23-28 Oct, 1972, Monte Carlo, pp 519-528
 26. TODD-POKROPEK AE: An investigation using Monte Carlo techniques and gaming theory into the values of digital radioisotope display system. In *Proceeding of Fourth Symposium on Medical Radioisotope Scintigraphy*. IAEA, 23-28 Oct, 1972, Monte Carlo, pp 705-723
 27. PAYNE JT, WILLIAMS LE, PONTO RA, et al: Comparison and performance of Anger cameras. *Radiology* 109: 381-386, 1973
 28. MORIN PP, MORIN JF, CAROFF J, et al: Caractérisation pratique de la linéarité de comptage d'une gamma caméra. *Int J Nucl Med Biol* 3: 101-103, 1976
 29. SORENSON JA: Deadtime characteristics of Anger cameras. *J Nucl Med* 16: 284-288, 1975
 30. MUNKNER T: Pulmonary function studies with radioisotopes. In *Proceeding of Dynamic Studies with Radioisotopes in Medicine* 1974. IAEA, 15-19 July, 1974, Knoxville, pp 319-343
 31. ADAMS R, ZIMMERMAN D: Methods for calculating the deadtime of Anger camera systems. *J Nucl Med* 14: 496-498, 1973
 32. ADAMS R, JANSEN C, GRAMES GM, et al: Deadtime of scintillation camera systems—definitions, measurements and applications. *Med Phys* 1: 198-103, 1974
 33. ADAMS R, HINE GJ, ZIMMERMAN D: Deadtime measurements in scintillation cameras under scatter conditions simulating quantitative nuclear cardiology. *J Nucl Med* 19: 538-544, 1978
 34. BITTER F, ADAM WE: A data acquisition and processing system for rapid dynamic investigations with a scintillation camera. In *Proceeding of Medical Radioisotope Scintigraphy*, 1972, Monte Carlo, pp 443-457
 35. MAKLER PT, EYMONTT MJ, BLOCH P, et al: Effect of small amounts of ¹³¹I on ^{99m}Tc detection by the scintillation camera. *J Nucl Med* 17: 1100-1101, 1976
 36. MORETTI JL, MENSCH B, GUEY A, et al: Comparative assessment of scintillation camera performance. *Radiology* 119: 157-165, 1976
 37. ROYAL HD, BROWN PH, CLAUNCH BC: Mobile gamma cameras: A comparative evaluation. *Radiology* 128: 229-234, 1978

**EASTERN GREAT LAKES CHAPTER
SOCIETY OF NUCLEAR MEDICINE
FIRST ANNUAL MEETING**

May 23, 1980

Sheraton Hotels

Niagara Falls, Ontario

The Eastern Great Lakes Chapter of SNM announces its First Annual Meeting to be held May 23, 1980, at Sheraton Hotels, Maple Leaf Village in Niagara Falls, Ontario, Canada.

The program will include continuing education courses to be given by: Dr. John McAfee, the SNM 1979 Paul C. Aebersold Award Winner on "Newer Concepts and Diagnostic Methods in Diseases of the Kidney;" Dr. David Weber on "Imaging Studies in Orthopaedics;" Dr. David Gilday on "Pediatric Nuclear Medicine in Perspective," and Dr. J. Calvin Brantley on "Management and Disposal of Radioactive Waste."

The technologist program will feature didactic lectures on "Computer Fundamentals and Their Clinical Nuclear Medicine Applications."

There will also be a presentation of contributed papers.

For further information contact:

Azu Owunwanne, Ph.D.
P.O. Box 620
Division of Nuclear Medicine
University of Rochester Medical Center
Rochester, NY 14642